Excitons and interband transitions in III-V semiconductor superlattices

P. M. Young, P. M. Hui,* and H. Ehrenreich†
Division of Applied Sciences, Harvard University, Cambridge, Massachusetts 02138
(Received 25 July 1991)

The fundamental optical absorption of $In_{1-x}Ga_xAs/In_{1-y}Al_yAs$ and $GaAs/Ga_{1-x}Al_xAs$ superlattices is calculated quantitatively using superlattice $\mathbf{K}\cdot\mathbf{p}$ theory. Electron-hole Coulomb interactions yielding excitons and interband-transition Sommerfeld enhancement are incorporated. These fast, nonvariational calculations yield optical structure within 2–3 meV and absolute absorption coefficients within 10% of experimental results for all but one of the twelve samples analyzed. Constituent bulk parameters and band offsets constitute the only input. Computer requirements are very modest. Calculations for different band offsets and other interface parameters using this versatile approach permit estimates of physically important quantities of relatively unexplored heterostructure systems, for example, II-VI superlattices.

I. INTRODUCTION

This theoretical study treats the effects of the electron-hole Coulomb attraction on the electronic and optical properties of III-V semiconductor superlattices (SL's) with emphasis on the remarkable quantitative agreement with the experimentally measured absolute optical-absorption spectra of several SL's. The present approach is an extension of previous work[1–3] which developed the $\mathbf{K}\cdot\mathbf{p}$ formalism to exploit the perfect periodicity of the SL heterostructure for determination of the electronic structure. Johnson[4] has briefly reported the transformation of the resulting SL crystal momentum representation (CMR) into a SL crystal coordinate representation (CCR) in connection with a calculation of the lowest bound exciton binding energies of the $GaAs/Ga_{1-x}Al_xAs$ SL system. In the present work, all Coulomb effects, including those on the continuum states, are treated to understand the excitation energies and the optical absorption in absolute terms.

The optical absorption has been generally calculated for the isolated-quantum-well (QW) regime.[5–8] Of notable exception is the work of Chu and Chang,[9,10] who have employed computationally intensive $\mathbf{k}$-space sampling techniques to study the SL absorption. Because of very significant computational simplification, the present work permits highly detailed quantitative comparison with experiment over broad energy ranges and for a variety of systems. In addition, it leads to verification (or prediction) of band offsets in systems like the II-VI SL's, where values are uncertain. For the III-V systems illustrated here, exciton peaks are shown to lie within 2–3 meV of their experimental locations and the overall absorption coefficient agrees within 10%.

As in previous work,[2] the SL band structure is obtained from the envelope function approach applied to a modified Kane model for the band structure of the constituent bulk materials. The only required input to the calculations consists of those parameters required to specify the Kane model in the constituents (gaps, heavy-hole masses, and a momentum matrix element), a valence-band offset which determines the lineup of the Γ_8 edges, and the index of refraction in the vicinity of the energy gap.

As described in Sec. II, which summarizes the formalism, the electron-hole Coulomb interaction is treated within an independent subband approximation that associates each exciton with a single conduction and a single valence band. This approach, together with a simple model for the SL Wannier functions, leads to an analytic form for the electron-hole interaction which permits solution for the exciton wave function without resorting to a variational approach. This nonvariational approach allows accurate determination of the exciton oscillator strength, and is not limited to bound states. Corrections involving the SL Sommerfeld factor also follow from the same formalism. A comparison with variationally obtained exciton binding energies is presented to verify the accuracy of the present approach.

In Sec. III the formalism is implemented and compared to experimental data published by several different groups. As already pointed out, agreement between experiment and theory is excellent. All of the major features displayed in the experiments are positively identified within the present theory. The final section discusses some implications of the present work with respect to band offsets and possible growth imperfections.

II. FORMALISM

This section summarizes the formalism for calculating the excitonic spectra and fundamental optical absorption of a SL. The one-electron band structure is described within the crystal momentum representation using the envelope function approach.[2] The SL wave function, depending on the SL band index L and wave vector $\mathbf{K}$, is expressed in terms of the bulk-basis Bloch functions $\langle \mathbf{r}|n,\mathbf{0}\rangle$ corresponding to bulk band n at $\mathbf{k}=\mathbf{0}$, and the envelope functions $F_n(L,\mathbf{K};\mathbf{r})$ by

$$\langle \mathbf{r}|L,\mathbf{K}\rangle = \sum_n F_n(L,\mathbf{K};\mathbf{r})\langle \mathbf{r}|n,\mathbf{0}\rangle \ . \quad (1)$$

$\mathbf{F}(L,\mathbf{K};\mathbf{r})$, having components $F_n(L,\mathbf{K};\mathbf{r})$, is obtained from

$$H^{\mathbf{k}\cdot\mathbf{p}}_{A(B)}(k_x,k_y,k_z\rightarrow -i\partial/\partial z)\mathbf{F}(L,\mathbf{K};\mathbf{r}) = E_L(\mathbf{K})\mathbf{F}(L,\mathbf{K};\mathbf{r}) \ . \quad (2)$$

$H^{\mathbf{k}\cdot\mathbf{p}}_{A(B)}$ is a $\mathbf{k}\cdot\mathbf{p}$ Hamiltonian modeling the band structure utilizing a modified Kane model including the uppermost six valence bands with finite heavy-hole mass and the lowest pair of conduction bands at $\mathbf{k}=\mathbf{0}$ in the bulk materials A and B. (A denotes the well and B the barrier material.) Equation (2) is solved for $\mathbf{K}=\mathbf{0}$ yielding SL zone-center energies, $E_L(0)$, and SL cell periodic envelope functions. These zone-center envelope functions determine the SL $\mathbf{K}\cdot\mathbf{p}$ matrix elements which are used to set up a secular equation whose solution at finite $\mathbf{K}$ yields the full band structure and momentum matrix elements $\langle L,\mathbf{K}|\mathbf{p}|L',\mathbf{K}\rangle$.

The optical absorption from the ground state $|G\rangle$ to excited states $|E\rangle$ associated with a photon of energy $\hbar\omega$ is

$$\alpha(E)=\frac{2\pi^2e^2\hbar}{n(E)mc}f_{EG}\rho(E) \ , \quad (3)$$

where m is the free-electron mass, $\rho(E)$ is the density of excited continuum states [$(1/V)\delta(E-\hbar\omega)$ for discrete states], $n(E)$ is the index of refraction, and $f_{EG}=2|\langle E|\mathbf{p}|G\rangle|^2/(mE)$ is the oscillator strength containing the momentum matrix element. The index will be approximated by an average n of the values for the constituent bulk semiconductors at the band gap.

In the absence of electron-hole interactions[11] $\langle E|\mathbf{p}|G\rangle=\langle L,\mathbf{K}|\mathbf{p}|L',\mathbf{K}\rangle$ and

$$\alpha(E)=\frac{2\pi^2e^2\hbar}{Vnmc}\sum_{L,L'}\sum_{\mathbf{K}}\frac{2}{m}\frac{|\langle L,\mathbf{K}|\mathbf{p}|L',\mathbf{K}\rangle|^2}{E_{L'}(\mathbf{K})-E_L(\mathbf{K})} \times\delta(E-E_L(\mathbf{K})+E_{L'}(\mathbf{K})) \ , \quad (4)$$

where V is the sample volume.

The electron-hole correlation due to the Coulomb interaction changes the absorption both qualitatively (discrete exciton peaks appear) and quantitatively (the continuum absorption is enhanced by the Sommerfeld factor). Because of the additional term in the Hamiltonian,

$$H_{e\text{-}h}=-e^2/\epsilon|\mathbf{r}_e-\mathbf{r}_h| \ , \quad (5)$$

where ϵ is the dielectric constant, and $\mathbf{r}_e$ and $\mathbf{r}_h$ are electron and hole coordinates, respectively, it will be most convenient to work in the SL-CCR.[4] A basis of SL Wannier functions is defined by

$$\langle\mathbf{r}|L,\mathbf{R}_\mu\rangle=N^{-1/2}\sum_{\mathbf{K}}e^{-i\mathbf{K}\cdot\mathbf{R}_\mu}\langle\mathbf{r}|L,\mathbf{K}\rangle \ , \quad (6)$$

where $\mathbf{R}_\mu$ is a lattice site. The Coulomb interaction couples *all* bands, but by imposing an independent subband approximation the coupling is restricted to single pairs of conduction and valence bands. All singlet excitonic states can then be expressed in a basis of two-particle Wannier states $|L,\mathbf{R}_\nu;L',\mathbf{R}_\mu\rangle$ corresponding to a hole in band L at $\mathbf{R}_\nu$ and an electron in band L' at $\mathbf{R}_\mu$.

The optical matrix elements are calculated for excitons having vanishing center-of-mass total momentum. The appropriate basis states

$$|\mathbf{R}_\rho;L,L'\rangle=N^{-1/2}\sum_{\mu}|L,\mathbf{R}_\mu-\mathbf{R}_\rho;L',\mathbf{R}_\mu\rangle \ , \quad (7)$$

depend only on the electron-hole relative coordinate $\mathbf{R}_\rho$. The exciton state is

$$|E^{LL'}_{\rm ex}\rangle=\sum_{\rho}U_{LL'}(\mathbf{R}_\rho)|\mathbf{R}_\rho;L,L'\rangle \ , \quad (8)$$

where $U_{LL'}$ is the exciton wave function which obeys the CCR equation[4]

$$\sum_{\rho'}\left[\frac{1}{N}\sum_{\mathbf{K}}e^{i\mathbf{K}\cdot(\mathbf{R}_\rho-\mathbf{R}_{\rho'})}[E_{L'}(\mathbf{K})-E_L(\mathbf{K})]\right]U_{LL'}(\mathbf{R}_{\rho'})-V(\mathbf{R}_\rho)U_{LL'}(\mathbf{R}_\rho)=E^{LL'}_{\rm ex}U_{LL'}(\mathbf{R}_\rho) \ . \quad (9)$$

Here $V(\mathbf{R}_\rho)$ is the direct Coulomb term

$$V(\mathbf{R}_\rho)=\int d\mathbf{r}_e\int d\mathbf{r}_h|\langle\mathbf{r}_e|L',\mathbf{R}_\rho\rangle|^2\frac{e^2}{\epsilon|\mathbf{r}_e-\mathbf{r}_h|} \times|\langle\mathbf{r}_h|L,\mathbf{0}\rangle|^2 \ . \quad (10)$$

The absorption in the presence of the Coulomb interaction will be modified with respect to Eq. (4) by the presence of the SL Sommerfeld factor and energetically discrete exciton peaks. Evaluation of the Sommerfeld factor and exciton spectra requires the solution of Eq. (9) for $U_{LL'}(\mathbf{R}_\rho)$. It can be determined both simply and accurately by approximating the Coulomb integral $V(\mathbf{R}_\rho)$ so as to be expressible in closed form. This calculation is facilitated by using a SL model band structure which is separable, parabolic in-plane, and tight-binding-like along the growth axis:

$$E_{L'}(\mathbf{K})-E_L(\mathbf{K})=E_g^{LL'}+\frac{\hbar^2\mathbf{K}_\parallel^2}{2\mu_\parallel^{LL'}} -\sum_{n=1}^{\infty}2W^{LL'}(n)[\cos(n\mathbf{K}_\perp d)-1] \ . \quad (11)$$

The directions $\parallel$ and $\perp$ are defined with respect to the growth planes and are identified with the x-y and z directions, respectively. $E_g^{LL'}$ is the interband gap given by $E_{L'}(0)-E_L(0)$, $\mu_\parallel^{LL'}$ is the reduced mass for the pair of

bands, and d is the SL period along the growth direction. The $W^{LL'}(n)$ are the hopping matrix elements involving nth nearest neighbors in the tight-binding model. For all but the thinnest barrier SL's ($L_B \lesssim 20$ Å), a nearest-neighbor model suffices. The parabolic in-plane approximation, which may be questionable for the valence-band structure in view of anticrossing effects in the closely spaced bands, is nevertheless adequate since only the reduced mass, which is dominated by the conduction bands, is required.

The Coulomb interaction between electron and hole cannot be treated within the normal effective-mass approximation in the growth direction since the SL unit cell in that direction is comparable to the bulk exciton Bohr radius. However, along the in-plane directions the effective-mass approximation for Wannier excitons, as used in the bulk problem, is appropriate.

The model employed is that introduced by Johnson,[4] who calculated very satisfactory binding energies for the lowest bound excitons of the GaAs/$Ga_{1-x}Al_xAs$ system within a SL-CCR framework. The electron and hole Wannier functions are modeled by one-dimensional rods of lengths L_e and L_h along the z axis. Within this model the Coulomb integral can be expressed in closed form:[12]

$$V(\mathbf{R}_\rho)\approx\frac{e^2}{\epsilon L_e L_h}\int_{-L_h/2}^{L_h/2}dz_h\int_{\rho_z-L_e/2}^{\rho_z+L_e/2}dz_e\frac{1}{[(z_e-z_h)^2+\rho_{xy}^2]^{1/2}}\ . \tag{12}$$

Here ρ_z and ρ_{xy} are the growth direction and in-plane components of the electron-hole relative coordinate $\mathbf{R}_\rho$, respectively (measured with respect to the hole position). For the present calculations the rod lengths, L_e and L_h, have been taken to be equal to the width of the well layer.[13] Figure 1 schematically illustrates the present model where electron and hole rods are localized in wells separated by ρ_z along the growth direction.

This model interaction reduces properly to the appropriate limiting cases, for example the two-dimensional hydrogenic limit in narrow quantum wells. The independent subband approximation is seen to fail when the quantum-well size is much larger than the exciton Bohr radius, a case that falls outside the parameter range of interest here.

The wave functions obtained as solutions of Eq. (9) correspond to bound excitons and resonant states having a continuum density of states. The momentum matrix element for singlet states with energy E_{ex} is given by

$$\begin{aligned}\langle E_{ex}|\mathbf{p}|G\rangle&=N^{-1/2}\sum_\rho U_{LL'}(\mathbf{R}_\rho)\sum_\mu\langle L,\mathbf{R}_\mu-\mathbf{R}_\rho|\mathbf{p}|L',\mathbf{R}_\mu\rangle\\&=N^{-1/2}\sum_\rho U_{LL'}(\mathbf{R}_\rho)\sum_{\mathbf{K}}e^{i\mathbf{K}\cdot\mathbf{R}_\rho}\langle L,\mathbf{K}|\mathbf{p}|L',\mathbf{K}\rangle\end{aligned} \tag{13}$$

[cf. Eqs. (7) and (8)].

In the Wannier exciton limit the Fourier transform,

$$g(\mathbf{K})=N^{-1/2}\sum_\rho e^{-i\mathbf{K}\cdot\mathbf{R}_\rho}U_{LL'}(\mathbf{R}_\rho) \tag{14}$$

of $U_{LL'}(\mathbf{R}_\rho)$, is strongly peaked about a particular in-plane $\mathbf{K}$ value, $\mathbf{K}=\mathbf{K}_\parallel$. For bound excitons $\mathbf{K}_\parallel\approx\mathbf{0}$. For the continuum states it is approximately $E_{ex}\approx\hbar^2K_\parallel^2/2\mu_\parallel^{LL'}$. For the range of parameters of interest the electron and hole are located in the same or nearly adjacent wells. The momentum matrix elements can therefore be averaged over the Brillouin zone along the $\mathbf{K}_\perp$ direction. Equation (13) can thus be expressed in terms of the SL momentum matrix element:

$$\begin{aligned}\langle E_{ex}|\mathbf{p}|G\rangle&=\sum_{\mathbf{K}}g(\mathbf{K})\langle L,\mathbf{K}|\mathbf{p}|L',\mathbf{K}\rangle\\&\approx N^{1/2}U_{LL'}(\mathbf{0})\langle L,\mathbf{K}_\parallel|\mathbf{p}|L',\mathbf{K}_\parallel\rangle\ .\end{aligned} \tag{15}$$

The Sommerfeld factor is defined as

$$\mathcal{S}(E)=N|U_{LL'}(\mathbf{0})|^2\ . \tag{16}$$

In the absence of electron-hole interactions $U_{LL'}(\mathbf{0})=N^{-1/2}$ and $\mathcal{S}(E)=1$.

Figure 2 illustrates the effects of the electron-hole interaction on the absorption of an (80-Å $In_{1-x}Ga_xAs$)/(114-Å $In_{1-y}Al_yAs$) SL. The absorption in the absence of electron-hole interactions, the contributions due to the bound exciton peaks, and the enhance-

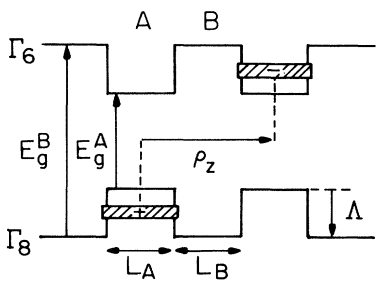

FIG. 1. Schematic illustration of relative band alignments and the representation of electron and hole Wannier functions by rods localized in the wells. A is the well material, B is the barrier material, and the Γ_8 valence-band edges are offset by Λ.

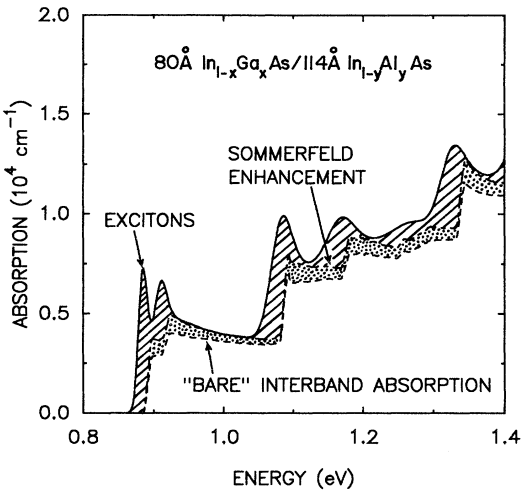

FIG. 2. The effect of the electron-hole interaction on SL absorption. Theory for the absorption of an (80-Å $In_{0.53}Ga_{0.47}As$)/(114-Å $In_{0.52}Al_{0.48}As$) superlattice is plotted with (solid line) and without (dashed line) electron-hole Coulomb interaction. Contributions due to Sommerfeld factor enhancement of continuum transitions (dotted region) and due to bound exciton peaks (crosshatched region) are separately identified.

ment due to the SL Sommerfeld factor for the continuum states are separately identified. The Coulomb interaction strengthens the overall absorption by about 20% and emphasizes the quasi-two-dimensional density of states steps with bound exciton peaks.

The behavior of the Sommerfeld factor is examined in more detail in Fig. 3 for the QW limit. The Sommerfeld factor is plotted as a function of energy above the band gap in exciton rydbergs $(E-E_G^{LL'})/R_H^{\rm ex}$, where $R_H^{\rm ex}=\mu_{\parallel}^{LL'}R_H/\epsilon^2$, for several values of the reduced well width, $w=L_A/a_B^{\rm ex}$. For the systems examined in this paper w is between 0.2 and 1.0. The 2D limit, $w=0$, corresponds to the case examined by Shinada and Sugano,[14] who found $\mathcal{S}(E)=e^{\pi\alpha}/\cosh(\pi\alpha)$, where $\alpha^{-2}=(E-E_G)/R_H^{\rm ex}$. The 3D limit, $\mathcal{S}(E)=\pi\alpha e^{\pi\alpha}/\sinh(\pi\alpha)$, is not obtained within the present formalism since it requires explicit consideration of the interaction of the subbands as they merge into a 3D density of states. The result obtained here is seen to differ from the ideal 2D limit even for monolayer confinements, $w\approx 0.03$, which motivated the work discussed in Ref. 14.

Figure 4 compares the results for QW exciton binding energies obtained from variational calculations with the results of the present formalism. Binding energies are in units of exciton rydbergs and well widths are normalized by the exciton radius $a_B^{\rm ex}$. The variational approach utilizes the effective-mass approximation along all axes; barrier layers are treated as step potential terms in the Hamiltonian. Separable solutions in Ref. 15 are obtained with trial wave functions that are products of profiles resembling envelope functions associated with particular conduction and valence subbands of the quantum well and trial in-plane profiles, e.g., decaying exponentials, that contain a variational parameter. The nonseparable trial wave function is a product of envelope functions and a decaying exponential in all directions in the well, including the growth axis. The resulting growth axis profile is no longer just a product of QW envelope functions, and thus cannot be uniquely associated with a single valence and single conduction band. Binding energies for the 1s exciton in exciton rydbergs, as obtained in Ref. 15 using separable and nonseparable variational models, are plotted together with results from the present formalism as a function of the reduced well width, w. The separable variational model yields results substantially identical to

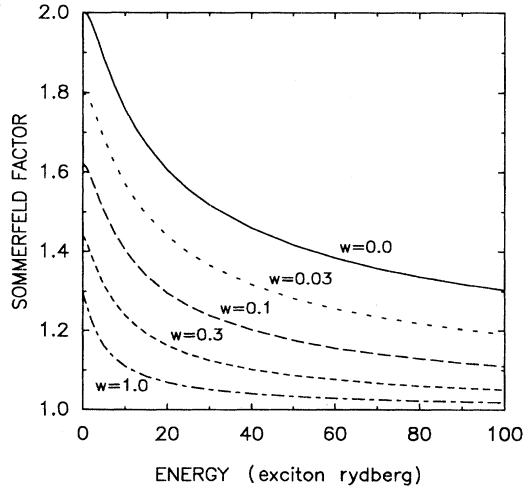

FIG. 3. Quantum-well Sommerfeld factor as a function of energy above the band edge (in exciton rydbergs) for several values of reduced well width, $w=L_A/a_B^{\rm ex}$, including the ideal 2D case $w=0$.

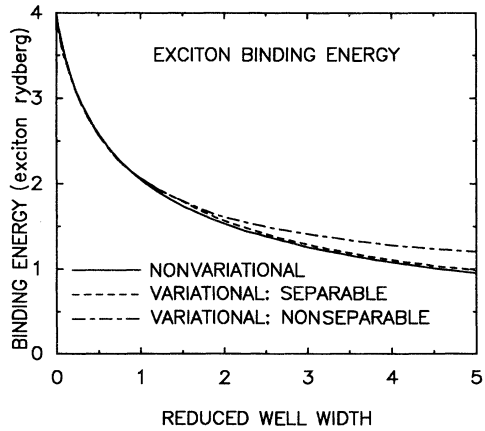

FIG. 4. Comparison of the present theory for exciton binding energies with variational calculations. The 1s exciton binding energy (in exciton rydbergs) is plotted as a function of the reduced well width (see text) for the present nonvariational theory (solid line), and for variational calculations based on separable and nonseparable trial wave functions.

the present formalism, which also agrees with the nonseparable model for reduced well widths, $w \leq 1.0$, the values of interest in the experimental results to be considered here. For wells of width significantly greater than the bulk exciton radius, the expected 3D bulk limit is obtained for the nonseparable model, but the separable and nonvariational binding energies slowly vanish because the separability approximation is not valid for very wide wells.

The above theory yields perfectly sharp exciton linewidths. We introduce a simple model based on monolayer well-width fluctuations to obtain a finite linewidth at low temperatures, ($T \approx 5$ K).[16] This model is based on the notion that a SL interface plane consists of islands containing materials of the adjacent layers. Excitonic transition energies are calculated for a SL of nominal layers width, and also for SL's whose layer widths vary by ± 1 monolayer while preserving the period, d. This generates a set of lines which are convoluted to produce a linewidth which is then multiplied by a single constant (of order unity and the same for all excitons calculated) chosen to best represent the experimental results.[17] This assumption concerning widths introduces the only arbitrary element into the present calculations. The model is supported by the fact that in the samples examined here, Gaussian line shapes match experiments more closely than Lorentzians, which would be expected if lifetime effects were responsible for the width at low temperature.[18–20]

III. IMPLEMENTATION OF FORMALISM

This section centers on comparison of the present theory with a broad selection of absolute optical-absorption spectra for the GaAs/$Ga_{1-x}Al_xAs$ and $In_{1-x}Ga_xAs/In_{1-y}Al_yAs$ systems. We have analyzed 12 sets of experiments by different groups and have obtained detailed agreement with 11. (The number of *absolute* measurements is actually quite limited.) In the $In_{1-x}Ga_xAs/In_{1-y}Al_yAs$ system the spectral range extends between 0.8 and 1.4 eV. Nonparabolic band effects must therefore be included. These are contained within the Kane model used to calculate the underlying band structures. Table I provides a summary of the parameters used to describe the relevant bulk semiconductors.

Experiment and theory are compared for the $In_{0.53}Ga_{0.47}As/In_{0.52}Al_{0.48}As$ system in Fig. 5.[24] The samples considered experimentally[21] have respective well and barrier widths of (34 Å)/(114 Å), (80 Å)/(114 Å), and (138 Å)/(115 Å), and are lattice matched. Strain effects, therefore, play no role. The present calculations include the contributions of all s symmetry bound excitons associated with each pair of bands. The 1s transition accounts for roughly 90% of the total oscillator strength of each family, and has the largest binding energy by a factor of about 6 for the present case. As a result none of the higher excitons is clearly resolved in the presence of the line broadening.

The major structure in the spectra is due to pairs consisting of transitions HH$n \rightarrow Cn$, and at slightly higher energy LH$n \rightarrow Cn$ for $n=1$, 2, 3, and 4. As n increases, the spacing between the pairs increases due to the different masses of the HH and LH bulk bands and the fact that the confinement energy goes roughly as n^2. *All* of the major features in the experiments, i.e., the absorption steps and excitons associated with the "allowed" transitions HH$n \rightarrow Cn$ and LH$n \rightarrow Cn$ and the associated absorption coefficients, are accurately predicted by the theory. In the case of the 138-Å well no fewer than eight such strong transitions exist in the photon energy range of 0.6 eV under examination.

Above 1.2 eV the theory is no longer quantitative. Results fall below experiment for all samples. This behavior is possibly associated with an Urbach tailing effect due to the InP substrate on which the samples are grown, and whose band gap, at 1.42 eV, limits the energy range which can be examined experimentally.

Optical-absorption experiments for the GaAs/$Ga_{1-x}Al_xAs$ system require etching off the GaAs substrate on which the sample is grown, since GaAs has strong absorption in the relevant energy range. As a result there are relatively few measurements of absolute op-

TABLE I. Summary of the bulk semiconductor $\mathbf{k}\cdot\mathbf{p}$ parameters and the valence-band offsets, Λ, used in the present calculations. E_g is the fundamental gap, Δ is the spin-orbit splitting, and m_{HH} is the heavy-hole mass along the [100] axis.

Parameter	$In_{0.53}Ga_{0.47}As$	$In_{0.52}Al_{0.48}As$	$Ga_{1-x}Al_xAs$
E_g (eV) (4 K)	0.813[a]	1.508[a]	$1.519+1.247x$
E_g (eV) (300 K)			$1.424+1.247x$[b]
Δ (eV)[c]	0.36	0.33	$0.34-0.06x$
m_{HH}/m	0.5	0.5	0.45
E_P (eV)[d]	22.0	22.0	24.0
Λ (eV)	0.200[a]		$0.374x$[e]

[a]Reference 21.
[b]Linear variation (Ref. 22) valid only for $0.0 < x < 0.45$ due to band-gap bowing.
[c]Linear interpolation of values in Ref. 23.
[d]E_P is defined as $(2/m)|\langle S|p_z|Z\rangle|^2$; its value is deduced from the $\mathbf{k}\cdot\mathbf{p}$ model using electron masses from Ref. 21 for the InAs alloys and $m_e = 0.067m$ for GaAs.
[e]Corresponding to a 70%-30% conduction- to valence-edge offset distribution between pure GaAs and the alloy.

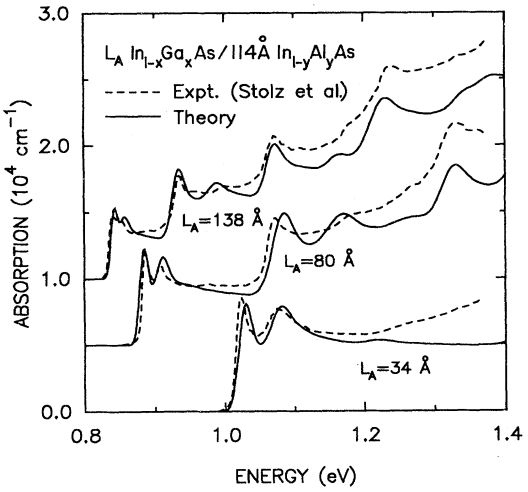

FIG. 5. Comparison of theory (solid lines) and experiment (dashed lines) for absorption in three samples in the $In_{0.53}Ga_{0.47}As/In_{0.52}Al_{0.48}As$ system with well and barrier widths as given. For clarity the curves for the 80-Å well were displaced upward by 0.5×10^4 cm^{-1}, and those for the 138-Å well by 1.0×10^4 cm^{-1}. Experimental data are from Ref. 21.

tical absorption for this system despite its importance. The lattice mismatch between GaAs and $Ga_{1-x}Al_xAs$ is $0.13x\%$ and the biaxial deformation potential is of order 1 eV. The effects of strain, which are at most one or two meV, may therefore be neglected.

Figure 6 compares theory to experiment[25] for a (116-Å GaAs)/(100-Å $Ga_{1-x}Al_xAs$) SL. While the agreement between theory and experiment is still excellent, it is not quite as satisfactory as that in the In-based system. The exciton peaks are also sharper in this system, which may be due in part to the absence of alloy compositional fluctuations in the well.[21] Note that the total-energy range

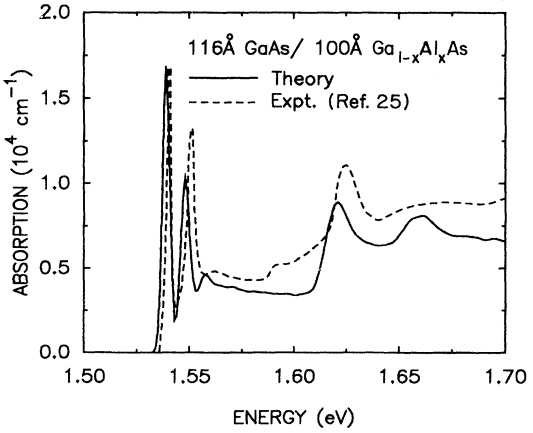

FIG. 6. Comparison of theory (solid line) and experiment (dashed line) for absorption in a (116-Å GaAs)/(100-Å $Ga_{0.75}Al_{0.25}As$) superlattice. Experimental data are from Ref. 25.

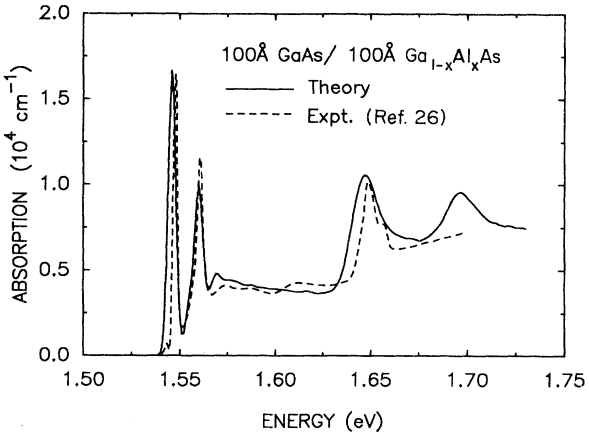

FIG. 7. Comparison of theory (solid line) and experiment (dashed line) for absorption in a (100-Å GaAs)/(100-Å $Ga_{0.7}Al_{0.3}As$) superlattice. Experimental data are from Ref. 26.

here is only 0.2 eV as opposed to the data in Fig. 5 which spanned a 0.6-eV range. The major optical structure is satisfactorily explained except for one feature, often called a "forbidden" transition. This feature, consisting of a step between the LH1$\rightarrow C1$ and HH2$\rightarrow C2$ peaks, will be discussed in Sec. IV.

A more recent spectrum[26] for a (100-Å GaAs)/(100-Å $Ga_{1-x}Al_xAs$) SL is shown in Fig. 7. The agreement with theory is better than that of Fig. 6, despite similarities in the layer widths. The forbidden transition is comparatively small. The experimental HH2$\rightarrow C2$ peak is seen to be split. This feature, which is not reproduced by the theory, arises because some oscillator strength is passed to the nominally forbidden LH1$\rightarrow C2$ transition via the $\mathbf{k}\cdot\mathbf{p}$ interaction of the nearly degenerate LH1 and HH2 bands. This occurs because of the $\mathbf{K}$ mixing in the exci-

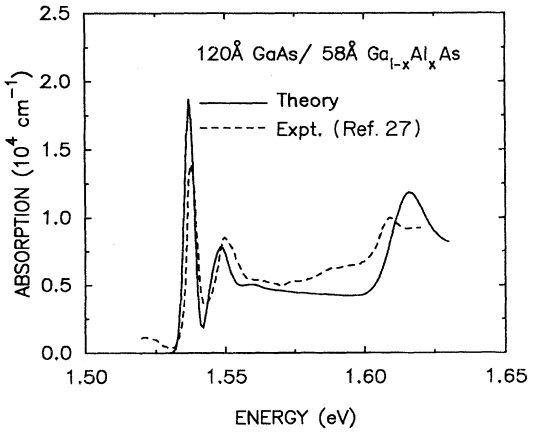

FIG. 8. Comparison of theory (solid line) and experiment (dashed line) for absorption in a (120-Å GaAs)/(58-Å $Ga_{0.71}Al_{0.29}As$) superlattice. Experimental data are from Ref. 27.

ton state which has been neglected here. The observed structure could be obtained theoretically using an improved optical matrix element in this spectral range.

Another sample,[27] (120-Å GaAs)/(58-Å $Ga_{1-x}Al_xAs$), is examined in Fig. 8. Here, satisfactory agreement is once again obtained. Note that this sample contains somewhat wider wells and narrower barriers than most others, yet agreement is still good.

IV. IMPLICATIONS

The above discussion has focused on two well-known III-V systems because of their intrinsic importance and because much of the most reliable data on SL and QW heterostructures exists for these materials. The quality of the agreement between experiment and theory suggests that absolute optical-absorption measurements may be useful as an aid in SL characterization. Here, we shall briefly describe two specific examples relevant to (1) determination of valence-band offsets, particularly for wide-band-gap II-VI systems where the offsets are largely unknown; and (2) characterization of effects resulting from possible growth defects.

To illustrate the dependence of absorption on the valence-band offset Λ we consider the 80-Å well In system SL described above. Absorption curves for offsets of $\Lambda=30$, 100, 200, and 300 meV are shown in Fig. 9. (Figure 5 shows the results corresponding to the solid line.) For $\Lambda=30$ meV, the HH1$\rightarrow C1$ and LH1$\rightarrow C1$ exciton peaks are not resolved from one another. This is to be expected for common-anion-rule (near zero) values of the offset (given that the system is strain free). As Λ increases from 30 to 100 meV the LH-HH degeneracy at $\mathbf{K}=\mathbf{0}$ is split and the lowest peaks separate. (The inset provides a magnification of this region.) For $\Lambda\approx 150$ meV this separation saturates at a value characteristic of perfect confinement. Between $\Lambda=30$ and 100 the HH2$\rightarrow C2$ and LH2$\rightarrow C2$ peaks appear and become resolved. For $\Lambda>150$ meV HH2 and LH2 become increasingly confined and stronger. This is particularly noticeable for the LH2$\rightarrow C2$ exciton peak. For $\Lambda\geq 200$ meV the HH2$\rightarrow C2$ exciton peak slowly falls in energy as HH2 is now fully confined and $C2$ begins to relax due to the decreasing value of the conduction-band offset.

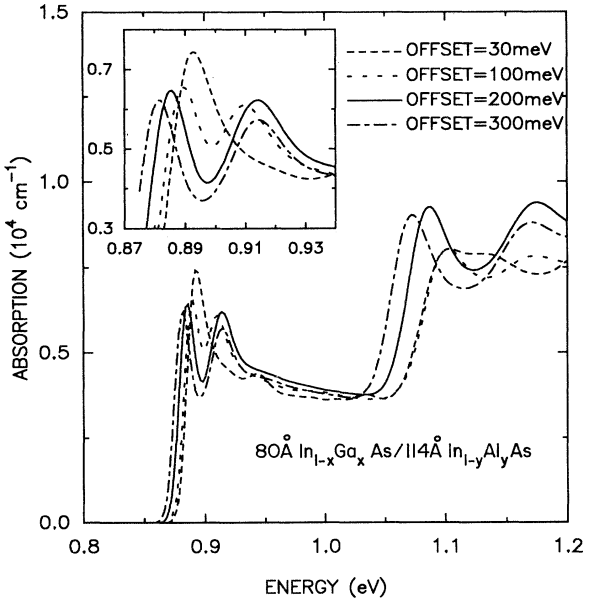

FIG. 9. Calculated fundamental optical absorption for several values of valence-band offset in an (80-Å $In_{0.53}Ga_{0.47}As$)/(114-Å $In_{0.52}Al_{0.48}As$) superlattice (see Fig. 5). The inset details the region of the spectrum around the HH1$\rightarrow C1$-LH1$\rightarrow C1$ doublet.

The above analysis supports the accepted value of Λ in the In system of 200 meV within an uncertainty of perhaps ± 30 meV. Thus it is expected that such calculations will be useful in characterizing less well understood systems. Work is presently under way to exploit this sort of analysis for the $Zn_{1-x}Cd_xSe$/ZnSe SL system, which is being examined as a candidate for an emitter in the blue-green region of the spectrum.[28]

Optical absorption may also be useful in characterizing SL growth defects. The so-called "forbidden" transition observed in the GaAs/$Ga_{1-x}Al_xAs$ sample is not explained by the present theory. Other calculations of SL absorption, such as those of Chu and Chang,[10] have also failed to explain the strength of this transition. This feature has been associated with the HH3$\rightarrow C1$ transition and used to infer properties of the bulk heavy-hole mass.[29] The size and shape of the optical absorption in this energy range is inconsistent with this interpretation. Furthermore, the magnitude of the structure is sample dependent. Work currently under way on the absorption of quantum wells in the presence of electric fields *suggests* that such a feature could be associated with intrinsic internal electric fields which could be introduced during the growth process. If correct, this interpretation would suggest that the effect of miscuts be examined more carefully.[30]

Not considered in this paper, but also relevant to the present theory, are superlattices having lattice-mismatched barriers and wells. These systems are complicated by effects such as the lifting of the Γ_8 degeneracy of the constituent bulk materials at the valence-band edge. Deformation potentials, which are less well determined in the II-VI's than in the III-V's, come into play, as does the question of the effect of strain on the valence-band offset. Mismatch effects have already been incorporated into the present calculations.

We emphasize that exploration of such effects is possible only because of the modest computer requirements for this type of systematic analysis. While the present theory does not necessarily improve upon the quality of the best calculations already published in the literature (although to our knowledge none of them compares with experimental absolute absorption coefficients), the approach *is* sufficiently versatile and accurate that a detailed survey of the dependence of properties of band offset and strain effects of potentially important systems on parameters such as alloy concentration is entirely feasible. This fact is of importance in candidate materials like $Zn_{1-x}Cd_xSe$/ZnSe, mentioned above, and related

systems such as CdTe/MnTe which are of interest as blue-green emitters and for which reliable experimental data are only now becoming available.

ACKNOWLEDGMENTS

We are grateful to N. F. Johnson for providing details not presented in Ref. 4 and for helpful discussions during the early stages of this work. This research was supported by the U.S. Joint Services Electronics Program (JSEP) through U.S. Office of Naval Research (ONR) Contract No. N00014-89-J-1023 and by the U.S. Defense Advanced Research Projects Agency (DARPA) through ONR Contract No. N00014-86-K-0033. One of us (P.M.Y.) would like to acknowledge the Fannie and John Hertz Foundation for partial financial support.

*Permanent address: Department of Physics, National Central University, Chung-li, Taiwan 32054, R.O.C.

†To whom all correspondence should be sent.

[1]N. F. Johnson, H. Ehrenreich, K. C. Hass, and T. C. McGill, Phys. Rev. Lett. **59**, 2352 (1987).

[2]N. F. Johnson, H. Ehrenreich, P. M. Hui, and P. M. Young, Phys. Rev. B **41**, 3655 (1990).

[3]N. F. Johnson, H. Ehrenreich, G. Y. Wu, and T. C. McGill, Phys. Rev. B **38**, 13 095 (1988).

[4]N. F. Johnson, J. Phys. Condens. Matter **2**, 2099 (1990).

[5]Y.-C. Chang and J. N. Schulman, Appl. Phys. Lett. **43**, 536 (1983).

[6]Y.-C. Chang and J. N. Schulman, Phys. Rev. B **31**, 2069 (1985). This reference and the previous reference consider the effects of well coupling on the band-to-band transitions, but not on the electron-hole interaction.

[7]G. D. Sanders and Y.-C. Chang, Phys. Rev. B **31**, 6892 (1985).

[8]G. D. Sanders and Y.-C. Chang, Phys. Rev. B **35**, 1300 (1987).

[9]H. Chu and Y.-C. Chang, Phys. Rev. B **36**, 2946 (1987).

[10]H. Chu and Y.-C. Chang, Phys. Rev. B **39**, 10 861 (1989).

[11]E. O. Kane, J. Phys. Chem. Solids **1**, 249 (1957). See also T. S. Moss and T. D. F. Hawkins, Infrared Phys. **1**, 111 (1961), who apply Kane's theory for the absorption to GaAs.

[12]P. M. Young, N. F. Johnson, P. M. Hui, and H. Ehrenreich (unpublished).

[13]Note that the rod lengths employed in the present calculations differ from those of Ref. 4. The present choice reproduces the results of variational calculations more accurately.

[14]M. Shinada and S. Sugano, J. Phys. Soc. Jpn. **21**, 1936 (1966).

[15]G. Bastard, E. E. Mendez, L. L. Chang, and L. Esaki, Phys. Rev. B **26**, 1974 (1982).

[16]C. Weisbuch, R. Dingle, A. C. Gossard, and W. Wiegmann, Solid State Commun. **38**, 709 (1981).

[17]In the limit of perfect square-well confinement the present method of assigning linewidths reduces to the model employed in Ref. 8 and elsewhere, where the linewidths are taken to be proportional to the squares of the quantum numbers, n, of the states.

[18]D. S. Chemla, D. A. B. Miller, and S. Schmitt-Rink, in *Optical Nonlinearities and Instabilities in Semiconductors,* edited by H. Haug (Academic, New York, 1988), pp. 91 and 92.

[19]J. S. Weiner, D. S. Chemla, D. A. B. Miller, T. H. Wood, D. Sivco, and A. Y. Cho, Appl. Phys. Lett. **46**, 619 (1985).

[20]D. A. B. Miller, D. S. Chemla, D. J. Eilenberger, P. M. Smith, A. C. Gossard, and W. T. Tsang, Appl. Phys. Lett. **41**, 679 (1982).

[21]W. Stolz, J. C. Maan, M. Altarelli, L. Tapfer, and K. Ploog, Phys. Rev. B **36**, 4301 (1987).

[22]H. C. Casey, Jr., J. Appl. Phys. **49**, 3684 (1978).

[23]P. Lawaetz, Phys. Rev. B **4**, 3460 (1971).

[24]The absorption coefficient α is approximately given by $I/I_0 = e^{-\alpha D}$, where I/I_0 is the ratio of transmitted to incident intensity, and D is the thickness of the sample. For multiple-quantum-well systems, D is often taken to be the total thickness of well material traversed. In this paper D is identified with the total sample thickness, i.e., as the sum of well *and* barrier thicknesses. See also the discussion in Ref. 25.

[25]W. T. Masselink, P. J. Pearah, J. Klem, C. K. Peng, H. Morkoç, G. D. Sanders, and Y.-C. Chang, Phys. Rev. B **32**, 8027 (1985).

[26]D. M. Huang, J.-I. Chyi, and H. Morkoç, Phys. Rev. B **42**, 5147 (1990).

[27]H. Iwamura, T. Saku, and H. Okamoto, Jpn. J. Appl. Phys. **24**, 104 (1985).

[28]P. M. Young, M. Ziegler, and H. Ehrenreich (unpublished).

[29]R. C. Miller, D. A. Kleinman, and A. C. Gossard, Phys. Rev. B **29**, 7085 (1984).

[30]F. Spaepen (private communication).